DOI: 10.1002/((please add manuscript number))
Article type: Communication

Mechanically defined microenvironment promotes stabilization of microvasculature, which correlates with the enrichment of a novel Piezo-1+ population of circulating CD11b+/CD115+ monocytes

*Aurelien Forget[#], Roberto Gianni-Barrera[#], Andrea Uccelli, Melika Sarem, Esther Kohler, Barbara Fogli, Manuele G. Muraro, Sandrine Bichet, Konrad Aumann, Andrea Banfi[§] and V. Prasad Shastri[§,]**

[#] These authors contributed equally

[§] These authors contributed equally

Dr. Aurelien Forget, Dr. Melika Sarem, Esther Kohler, Prof. Dr. V. P. Shastri
Institute for Macromolecular Chemistry, University of Freiburg, 79104 Freiburg, Germany
Dr. Aurelien Forget
Science and Engineering Faculty, Queensland University of Technology, Brisbane 4001, Queensland, Australia
Dr. Roberto Gianni-Barrera, Andrea Uccelli, Barbara Fogli, Dr. Manuele G. Muraro, Dr. Andrea Banfi
Department of Biomedicine, University Hospital Basel, Basel 4056, Switzerland.
Dr. Roberto Gianni-Barrera, Andrea Uccelli, Dr. Manuele G. Muraro, Dr. Andrea Banfi
Department of Surgery, University Hospital Basel, Basel 4056, Switzerland
Dr. M. Sarem, Prof. Dr. V. P. Shastri
BIOSS Centre for Biological Signaling Studies, University of Freiburg, 79104 Freiburg, Germany
Helmholtz Virtual Institute on Multifunctional Biomaterials for Medicine, Kantstr. 55, 14513 Teltow, Germany
Email: prasad.shastri@gmail.com
Dr. Sandrine Bichet
Friedrich Miescher Institute for Biomedical Research, Basel 4058, Switzerland
Dr. Konrad Aumann
Institute for Surgical Pathology, Medical Center – University of Freiburg, Faculty of Medicine, University of Freiburg, Germany

Keywords: therapeutic angiogenesis; mechanobiology, Piezo-1; vessel stabilization; carboxylated agarose

Abstract: Vascularization is a critical step in the restoration of cellular homeostasis. Several strategies including localized growth factor delivery, endothelial progenitor cells, genetically engineered cells, gene therapy, and pre-vascularized implants have been explored to promote re-vascularization. But, long-term stabilization of newly-induced vessels remains a challenge. It has been shown that fibroblasts and mesenchymal stem cells can stabilize newly-induced vessels. However, whether an injected biomaterial alone can serve as an instructive environment for angiogenesis remains to be elucidated. We report that appropriate vascular branching, and long-term stabilization can be promoted simply by implanting a hydrogel with stiffness matching that of fibrin clot. We have identified a unique sub-population of circulating $CD11b^+$ myeloid and $CD11b^+/CD115^+$ monocytes that express the stretch activated cation channel Piezo-1 which is enriched prominently in the clot-like hydrogel. These findings offer evidence for a mechanobiology paradigm in angiogenesis involving an interplay between mechano-sensitive circulating cells and mechanics of tissue microenvironment.

In peripheral artery disease, establishment of new vasculature is critical for rescuing the ischemic tissue and is a necessary step for successful engraftment of a transplanted tissue/organ. Therapeutic angiogenesis, is a clinical strategy pioneered by Takeshita and Isner, to induce new blood vessels (collateral vessels) in ischemic tissues from existing vasculature using external cues[1]. The repertoire of external cues range from localized delivery of proangiogenic factors (vascular endothelial growth factor (VEGF)[2], fibroblast growth factor(FGF)[3]), endothelial progenitor cells[4], cells genetically engineered to secrete a single or a combination of proangiogenic factors[5], and gene therapy[6]. More recently hypoxia-based strategies including pre-conditioning of mesenchymal stem cells (MSCs) to hypoxia before transplantation[7], and gene therapy to locally engineer cells to express hypoxia inducible factor-1α have also been explored. One of the challenges with local delivery of proangiogenic

signals, such as VEGF, is that the sprouting and maturation of new vessels into normal or aberrant (tumor-like vessels) depends on the formation of precise concentration gradients in the vessel microenvironment. These depend both on the combination of different isoforms with varying affinity for extracellular matrix and their local concentration[8], which are very difficult to modulate and control. After injury, endothelial cells (ECs) lose their quiescence and get primed and become sensitive to external pro-angiogenic cues. Maintenance of the neovasculature is however vital for vascular homeostasis. In this regard, perivascular cells i.e., pericytes and vascular smooth muscle cells play a critical role *in vivo* in not only providing scaffolding but also paracrine signaling necessary for blood vessel sprouting and maturation[9], In therapeutic angiogenesis, vessels often fail to mature and regress over time[10] due to inadequate recruitment of appropriate support cells, and it has been shown that co-culturing of ECs with MSCs[11] or fibroblasts[12] prior to implantation can promote stabilization of new blood vessels and their perfusion. Nonetheless, strategies to promote maturation and stabilization of neovasculature through endogenous mechanisms could be more translatable.

During angiogenesis, ECs express αv family of integrins, which are transmembrane proteins that specifically bind to the arginine-glycine-aspartic acid (RGD) sequence found in many ECM molecules including collagen, fibronectin, and vitronectin[13]. Since integrins are also anchored to the actin cytoskeleton of the cell[14], they function as mechanotransducers and assist the cells in perceiving the mechanics of the ECM; and it has been shown that integrin signaling is necessary for both EC survival and proliferation[15]. In spite of this compelling evidence linking mechanical cues to EC function, the impact of the ECM mechanical properties on blood vessel sprouting and maturation remains unknown. We had recently demonstrated in vitro that soft carboxylated agarose (CA) hydrogel in combination with RGD-signaling and soluble pro-angiogenic signals (VEGF, FGF-2 and phorbol-12-myristate 13-acetate (PMA))

can promote the apical-basal polarization of ECs and their organization into free-standing multicellular lumens[16]. Encouraged by this observation, in this study we inquired if the mere introduction of CA hydrogels of appropriate mechanical properties could be sufficient to promote maturation and stabilization of neovasculature in vivo. Specifically, we chose a 2 % w/v solution of CA with 28% and 60% carboxylation as they yielded gels of two distinct stiffness (5 kPa (stiff gel) and 0.5 kPa (soft gel), respectively) that mimic the mechanical properties of gastrocnemius lateralis muscle, which has been reported be around to around 11 kPa which corresponds to a shear modulus of around 3-4 kPa [17], and fibrin network of blood clot (0.06 – 0.6 kPa)[18]. To ensure mechanical coupling of ECs with the gel and to exploit the known benefits of RGD signaling in maintenance of EC function, the CA backbone was functionalized with a peptide presenting the GGGGRGDSP sequence in the N-terminus using aqueous 1-Ethyl-3-(3-dimethylaminopropyl)carbodiimide (EDC) chemistry, as previously described[16]. Since RGD ligand density is known to impact cell-biomaterial interaction, the reaction conditions were optimized to ensure the same density of RGD (11.6±0.9 % of disaccharide repeat units) in both CA gels.

Mechanically-defined carboxylated agarose hydrogels support vascular ingrowth and recruitment of mural cells:

In order to evaluate the potential angiogenic response of CA hydrogels, four formulations: soft and stiff gels with and without soluble growth factors supplementation (GFs: 2.5 ng/mL of each VEGF, FGF-2 and PMA, i.e. 0.125 ng of each/50 µL of gel injected in the muscle) were implanted into SCID mice gastrocnemius muscles, a target tissue relevant for peripheral artery diseases. The concentration of the growth factors in this cocktail was based on our previous finding that they can promote organization of endothelial cells into lumens in vitro[16]. Hematoxylin and Eosin staining revealed that after 2 weeks, gels were evident in all conditions

and invoked no adverse inflammatory response or foreign-body reaction with collagenous capsule formation, and thus were well tolerated by the muscle tissue (**Figure 1a-d**). The ability of the CA gels to support the ingrowth of micro-vessels into its avascular environment was investigated by immunofluorescence and confocal microscopy. All CA gel environments, irrespective of GF supplementation were efficiently invaded by newly formed micro-vessels, physiologically associated with mural cells, i.e. pericytes (positive for nerve/glial antigen 2 (NG2) and negative for α-SMA), and smooth muscle cells (positive for α-SMA) (**Figure 1e-h**). The vessel diameters (**Figure 1i**) were similar in all conditions and the degree of angiogenesis within the gel as measured by the vessel length density (VLD), i.e. the total length of vessels in a given area, was statistically similar between soft and stiff gel formulations regardless of GF supplementation (stiff vs soft and stiff +GF vs soft +GF) (**Figure 1j).** It is well established that functionality of micro-vascular networks correlates with branching (short segment length, which depends on the number of branch points in relation to the total amount of vascularity)[19] and a moderate diameter in the range of capillaries (5-10 µm). In this regard, the shortest average segment length interestingly was achieved in the soft gel environment in absence of GF, while in their presence segment length was the highest of all conditions, though not statistically significant (soft = 207.8±48.2 µm, soft+GF = 428.5±103.6 µm, stiff = 277.1±41.3 µm, stiff+GF = 278.5±55.6 µm, $p<0.01$ soft vs stiff, $p<0.05$ soft vs stiff+GF and $p=0.087$ soft vs soft+GF) (**Figure 1k**). In order to assess if the capacity of CA gels to support vascular ingrowth could be further improved, CA gels were supplemented with Matrigel (0.01 % w/v), a biomaterial known to stimulate angiogenesis due to its optimal combination of basal lamina extracellular matrix and rich content of natural angiogenic growth factors[20]. The choice of the Matrigel concentration was based on our prior studies showing that at this concentration, Matrigel can support EC tubular organization while having no impact on the mechanical properties of the CA gel[16]. After two weeks, we found that Matrigel addition did

not affect the integration of the gels in the muscle and did not confer any noticeable benefits over CA gels supplemented with GF and yielded capillary networks that were less branched, as evidenced by longer vascular segments (**Figure S1a-g**). Taken together, these data suggest that while both soft and stiff gels were equally effective in inducing initial vascular ingrowth, the addition of growth factors or Matrigel does not confer any significant advantage, but the gel stiffness appears to matter for vessel branching.

Microenvironment with mechanical properties similar to blood clot uniquely promotes long-term stabilization and patency of newly formed vascular structures: To be therapeutically useful, newly induced vascular structures must stabilize, i.e. persist long-term without regression. Since, newly induced vessels require about 4 weeks to become independent of further angiogenic stimuli and persist indefinitely[8], the fate of initially induced vascular structures (vasculature diameter, length density and branching) within CA gels with and without GF was characterized 7 weeks after implantation (**Figure 2a-d**). Since GF and Matrigel supplementation yielded similar outcomes, the condition with GF alone was included in this experiment in order to account for their role during initial vessel induction.

We made a compelling finding that although vessel diameter was similar among all groups (**Figure 2i**), vasculature within the stiff gels in the absence of GF showed a significant regression of 50 % of VLD when compared to the 2-week time point from 3.4±0.3 to 1.7±0.2 mm/mm^2 ($p<0.0001$) (**Figure 2j**). In contrast, within soft gels similarly deprived of GF not only was the vessel regression arrested, but a further 125% expansion of the vessel network was observed (VLD 2wk = 3.6±0.3 mm/mm^2, $p<0.0001$ vs 7wk = 8.1±1.3 mm/mm^2) resulting in considerably denser vascularity than within the stiffer gels **(Figure 2a-h)**. Further analysis revealed that within the stiff gels vessel regression was accompanied by a reduction in network branching, with a 40% increase in vascular segment length from 277.1±41.3 µm to 465.2±73.7

µm; whereas within the soft gels capillary networks further increased their branching degree compared to the 2-week time-point regardless of GF supplementation (segment length soft = 117.4±10.5 µm and soft +GF = 55.3±18.5 µm) (**Figure 2k**). Once again as in the case at 2 weeks GF supplementation neither increased vessel density within soft gels nor did it promote stabilization (VLD 7wk soft+GF = 7.2±1.5 mm/mm^2 vs soft = 8.1±1.3 mm/mm^2, p = n.s.; VLD 2wk soft+GF = 5.0±0.8 mm/mm^2 vs soft = 4.7±0.3 mm/mm^2, p = n.s.). Pericytes have been shown to play a crucial role in vessel stabilization, both through secreted and cell contact-dependent signals [21]. While vessels within the stiff gels were scarcely associated with mural cells of any kind (**Figure 2a-b** and **e-f**), vessel networks within the soft gels resembled normal muscle capillaries and were associated with NG2+ pericytes (**Figure 2c-d**), which established tight cell-to-cell contacts with the endothelium (**Figure 2g-h**). Quantification of pericyte coverage (ratio of vessel length associated with NG2+ pericytes/total vessel length) showed that vascular networks within the soft gels were greater than 5-fold more mature compared to those within the stiff gels (soft+GF = 0.76±0.08 vs stiff+GF = 0.13±0.03, p<0.001; and soft = 0.73±0.05 vs stiff = 0.14±0.02, p<0.01; **Figure 2q**). Considering the large body of work highlighting the challenges associated in controlling complex set of variables (i.e., dose distribution in tissue, duration of stimulation, growth factor splice variants and their combinations) that impact the induction of physiological angiogenesis by growth factor delivery (either as delivered proteins or by gene therapy)[8, 22, 23], the ability of a mechanically defined biomaterial environment to induce robust and persistent normal angiogenesis independently of growth factor delivery, as shown here, is particularly attractive.

Newly formed vessels require functional perfusion by the systemic circulation in order to stabilize and persist, as lack of flow in a nascent vascular structures, regulated by pre-capillary arteriole sphincters, is a mechanism by which vascular networks prune redundant vessels and

adapt to the metabolic needs of the tissue[24]. Therefore, the establishment of functional blood flow in newly induced vascular structures was assessed by intravenous injection of biotinylated tomato lectin that binds the luminal surface of blood vessels and marks only vessels that are functionally perfused by systemic circulation[22]. Quantification of lectin perfusion showed that vessels in all conditions were well perfused (~ 70% of lectin+ endothelial structures), with the stiff gels showing a moderate reduction to ~ 50% (**Figure 2l**). This provided evidence that the RGD-modified CA gels support formation of fully functional vascular networks. Since Masson trichrome staining (**Figure S2**) revealed that hydrogels persist at the site of implantation even after 7 weeks, induce no foreign-body reaction as assessed by the absence of a collagenous capsule, and support efficient infiltration of host cells, the gels can be considered well integrated in muscle tissue. However, since SCID mice while having a fully functional innate immunity and inflammatory responses, lack B and T lymphocytes, the fate of the gels in immunologically fully competent subjects need to be further assessed in a future study. Taken together, these data suggest that: a) soft CA gel with mechanical properties similar to fibrin clot specifically promotes new vessel stabilization, yielding long-term persistent and mature (pericyte-associated) micro-vascular networks with the most optimal functional features of high density and branching complexity, and b) GF supplementation does not improve the long-term angiogenic effect that are already imposed by the mechanical environment of the gels. Therefore, the observed effects may be attributed to the presence of RGD-modified CA gel environment.

Circulating myeloid cells are enriched preferentially in soft hydrogel microenvironment: In order to elucidate a biological basis for our observations we explored two scenarios that could promote neo-vascularization and vessel stabilization namely: (1) differences in proliferation of endothelial cells in the gels, and/or (2) recruiting of circulating support cells.

We investigated endothelial proliferation by immunostaining for Ki67, which marks the nucleus of cells in all phases of the cell cycle (G_1, S, G_2, and M), excluding quiescent ones (G_0)[25]. Quantification of Ki67+ endothelial nuclei showed that vascular networks in all gel compositions were essentially quiescent after 7 weeks, with at least 98% of ECs in G_0 phase (**Figure 2m-p and 2r**). This is consistent with previous findings that in fully normal angiogenesis induced by VEGF 93% of ECs are in the G_0 phase already after 1 week[26].

It has been shown that circulating myeloid cells can be recruited to sites of active angiogenesis and play a role in both maturation and stabilization of new vessels[27]. In particular, a specific population of CD11b+ monocytes called Neuropilin-Expressing Monocytes (NEM), which express Neuropilin-1 (Nrp1), a co-receptor for VEGF and Semaphorin3A co-receptor, has been recently found to accelerate new vessel stabilization by directly activating TGF-β1 signaling[22], and indirectly by promoting pericyte recruitment through PDGF-BB secretion[28]. We therefore investigated whether the long-term stabilization of the capillary networks by the soft gel could relate to a differential enrichment of myeloid cells and specifically pro-maturative $CD11b^+$ monocytes. Immunofluorescent staining of cryo-sections of the gels two weeks following implantation revealed that the population of CD45+ myeloid cells was about 40% higher in the softer versus the stiffer gel environment (476.9±37.7 vs 333.8±44.7 cells/field, $p<0.01$; **Figure 3a-c)**, but the enrichment of CD11b+ cells were similar in both gel environments (**Figure 3d-f**).

Mechanically defined microenvironments sequester a unique $CD11b^+$ sub-population expressing the stretch-activated cation channel Piezo-1: Mechanobiology, the paradigm in which mechanical stimuli are translated in biological signals through mechanotransduction elements, has a prominent role in the organization of cells[16] and interaction between cell

populations[29]. In addition to signaling via αv integrins, a family of RGD-binding integrins[30], the stretch-activated ion channel Piezo-1[31] – an integrin activating transmembrane protein, has been shown to have critical role in angiogenesis[32]. Piezo-1 has also been implicated in cell-cell interactions[29] and has been shown to be inherently mechanosensitive[33]. Since the observed differences in the maturation and persistence of vessels are clearly correlated to the vastly differing stiffness of the two gels we inquired if the cells recruited into the gel environment express Piezo-1. Immunofluorescence staining identified for the first time a hitherto unknown population of $CD11b^+$ myeloid cells expressing Piezo-1 (**Figure 4a-b**), which was significantly more frequently found in the softer than in the harder hydrogels, representing 93.1±1.4% of the total $CD11b^+$ cells in the soft gels vs 71.8±2.4% in the stiff gels ($p<0.0001$; **Figure 4c**). Since CD11b is also expressed by neutrophils, which can also be recruited to sites of biomaterial implantation up to 2 weeks[34], we analyzed whether monocytes and/or neutrophils were present in the gels two weeks after implantation by H&E staining by exploiting their easily recognizable and characteristic nuclear morphologies. As shown in **Figure S3**, both cell types could be identified in gels of both stiffnesses. Based on this finding we further characterized the identity of the $CD11b^+$/Piezo-1^+ cells by staining for co-expression of CD11b with the specific markers CD115 for monocytes and Ly6G for neutrophils[35], and quantified their relative enrichment in the soft vs stiff gels. Interestingly, we identified novel Piezo-1^+ sub-populations of both monocytes and neutrophils in both 0.5 and 5 kPa gels (**Figure 4d-g**). However, quantification of the two populations revealed that only Piezo-1^+ monocytes were significantly enriched by about 1.7-fold in soft vs hard gels (0.5 kPa=40.6±4.6% of total $CD11b^+$ cells vs 5 kPa=24.4±2.6%, $p<0.01$; **Figure 4h**), whereas Piezo-1^+ neutrophils were similarly frequent in the two conditions (0.5 kPa=25.4±3.9% vs 5 kPa=19.5±2.0%, p=n.s.; **Figure 4h**).

In order to ascertain if Piezo-1$^+$ myeloid populations exist in the circulation and are enriched into the gels, or if Piezo-1 expression is induced upon exposure to the gel microenvironment, both mouse and human peripheral blood mononuclear cells were analyzed using flow cytometry. Human cells were also analyzed in order to establish the validity of the results in a translational perspective. A population of Piezo-1-expressing CD11b$^+$ cells was identified in the circulation of both mouse and healthy human donors (**Figure 4i-j**), with surprisingly similar frequency, accounting for 35.0±2.2% and 35.1±9.1% of total CD11b$^+$ cells respectively. However, further separation of the CD11b$^+$ population between monocytes and neutrophils, based on mutually exclusive expression of CD115 and Ly6G (mouse) or CD14 and CD66b (human), showed that a Piezo-1$^+$ sub-population could be found only in circulating monocytes, but not in neutrophils (**Figure 4k-l**), with similar frequency in both mouse and human blood (46.9±18.5% and 48.5±15.9% of total monocytes, respectively; **Figure 4m-n**).

Therefore, these data suggest that a population of mechano-sensitive CD11b$^+$/CD115$^+$/Piezo1$^+$ monocytes exist in normal circulation and that they can accumulate in CA hydrogels in differential manner based on their mechanical properties. The basis for this enrichment of CD11b+/Piezo-1+ population within CA gels could be either due to increased survival or retention or both and needs further investigation. On the other hand, mechanosensitive neutrophils could not be found in the circulation, but were observed in the CA gels, suggesting the possibility that Piezo-1 expression in this case may be mainly induced by the gel environment. The role of immune cells in regenerative medicine is an emerging theme. It has been recently shown that T helper 2 (Th2) lymphocytes, which comprise adaptive immunity play an important role in facilitating muscle tissue regeneration by ECM-based biomaterials[36]. Interestingly, our data show that the purely angiogenic effect of vessel stabilization by a mechanically defined environment does not require adaptive immunity, as this is lacking in the SCID mice. It is worth noting that in pulmonary inflammation recruitment of CD11b$^+$ myeloid

290 cells have been found to be critical in the homing of activated Th2 lymphocytes and
291 orchestration of an adaptive immune response[37]. Since the introduction of the gel in the
292 muscle environment is bound to invoke an inflammatory response, the presence of $CD11b^+$
293 cells could be a consequence of an inflammatory response. Considering these observations and
294 the recently identified functions of $CD11b^+$ monocytes in regulating the stabilization of newly
295 induced vessels[22], the novel population of $CD11b^+/CD115^+/Piezo1^+$ monocytes identified
296 here may represent the link between the mechanics and angiogenic properties of hydrogels and
297 represents a novel direction for future efforts in developing systems and pharmacological
298 agents for therapeutic angiogenesis.
299
300 **Materials ad Methods**
301 **Gels preparation and characterization**
302 Native agarose (1 g) (Merck, Darmstadt, Germany) was transferred into a 3-necked round-
303 bottom flask equipped with a mechanical stirrer and pH-meter (WTW, Weilheim, Germany),
304 and dissolved in deionized water at a concentration of 1% w/v by heating to 90 °C. The flask
305 was cooled down to 0 °C, using an ice bath, under vigorous mechanical stirring in order to
306 prevent gelation of the agarose, and the reactor was charged with 99% (2,2,6,6-
307 tetramethylpiperidin-1-yl)oxyl (TEMPO) (20.6 mg, 0.16 mmol), NaBr (0.1 g, 0.9 mmol), and
308 NaOCl (2.5 mL, 15% solution) all obtained from Sigma Aldrich (Steinheim, Germany). As the
309 reaction occurs, the solution becomes acidic. The pH of the solution was maintained at 10.8 by
310 dropwise addition of NaOH (0.1M) (Sigma-Aldrich Chemie GmbH, Steinheim, Germany)
311 throughout the duration of the reaction. The degree of carboxylation was back calculated by
312 using the volumes of NaOH (0.1 M) solution added during the reaction. The reaction was
313 quenched by the addition of $NaBH_4$ (0.1 g) (Sigma-Aldrich Chemie GmbH, Steinheim,
314 Germany), following which the solution was acidified to pH 8 (0.1mHCl) and stirred for 1 h.

The modified agarose was then precipitated by the sequential addition of NaCl (12 g, 0.2 mol) and ethanol (500 mL) (technical grade). The product was collected by vacuum filtration using a fritted glass funnel and then washed using ethanol (500 mL). The ethanol, catalyst, and salts were removed by extensive dialysis against water for 2 days with replacement of the water every 12 h. The modified agarose was then freeze-dried on a Beta 2−8 LD (Martin Christ Gefriertrocknungsanlagen GmbH, Osterode am Harz, Germany) overnight to yield a white solid. The degree of carboxylation was verified by the appearance of peaks associated with aliphatic carboxylic acid groups via FTIR (KBr) (νc=o: 1750 cm−1) (Bruker Optics, Ettlingen, Germany) and NMR 300 Mhz (^{13}C: 180 ppm) (Bruker BioSpin, Rheinstetten, Germany). The number average molecular weight of CA was determined as described earlier[16] and was in the range of 83,000 – 95,000.

Carboxylated agarose mechanical properties

Rheology experiments were performed with a Physica MCR 301 (Anton Paar, Wundschuh, Austria) equipped with a Peltier cell to control the temperature and the experiment was performed with a plate geometry PPR25 (Anton Paar, Wundschuh, Austria). Samples in deionized water were prepared by heating at 90 °C for 10 min until a clear solution was obtained. The liquid was then poured on the rheometer plate and the following sequence was used to determine the shear modulus: cool down from 80 °C to 5 °C in 30 min, 30 min equilibration at 5 °C to allow the gel to form, followed by heating to 37 °C and equilibration for 30 min prior to measuring G′ and G″ by increasing the rotation frequency from 0.01 rad/s up to 10 rad/s with a 1% deformation. The G′ of the gel was determined at 1 Hz shear frequency.

Carboxylated agarose RGD functionalization

Functionalization of CA with the RGDSP (Peptides International, Louisville, Kentucky, USA) peptide was performed using 1-ethyl-3-(3-dimethyl-aminopropyl)carbodiimide (EDC) (Sigma-Aldrich Chemie GmbH, Steinheim, Germany) coupling chemistry. CA was sterilized overnight in 70% ethanol, and the ethanol was re- moved by extensive dialysis against water. The sterile CA was freeze-dried overnight to yield a white solid. CA (30 mg, 0.25 µmol) was dissolved in MES sterile buffer (Sigma-Aldrich Chemie GmbH, Steinheim, Germany) and an excess EDC (210 mg, 1.3 mmol) was added and the solution stirred for 30 min. Following this the peptide was added (500 µg, 0.66 µmol for the CA-60 gels and 1 mg, 1.33 µmol for the gels) and the solution stirred for an additional 2 h at room temperature. Unreacted reagents were removed by dialysis against water. RGD incorporation was verified using elemental analysis Vario EL (Elementar Analysen systeme GmbH, Langenselbold, Germany) equipped with a thermal conductivity detector and an adsorption column for CO_2 at 110 °C and H_2O at 150 °C. All samples were accurately weighed to 3 mg before measurements and the percentage of nitrogen was used to calculate the peptide attachment. It was found that 11.6 ± 0.9 % of the repeat units where functionalized on both CA-28 and CA-60.

Gels implantation in vivo

Gels were implanted into 10-15 week old immune-deficient SCID CB.17 mice (Charles River Laboratories, Sulzfeld, Germany). Animals were treated in accordance with Swiss Federal guidelines for animal welfare, and the study protocol was approved by the Veterinary Office of the Canton of Basel-Stadt (Basel, Switzerland; Permit 2071). Gels were pre-loaded in 1 ml syringes and kept on ice (~ 4 °C) until injection. Fifty µl of cold PBS (Sigma-Aldrich Chemie GmbH, Steinheim, Germany) followed by 50 µl of cooled gels were implanted along the midline of both the *medialis* and *lateralis* portions of Gastrocnemius leg muscle in a standard

caudo-rostral direction, using a syringe with a $29^1/_2$G needle (Becton Dickinson, Allschwil, Switzerland). Gels supplemented with growth factors were loaded with 50 ng/mL of each vascular endothelial growth factor (VEGF), fibroblast growth factor 2 (FGF-2) both from R&D Systems (Minneapolis, USA) and phorbol-12-myristate 13-acetate (PMA) from Sigma Aldrich (Munich, Germany).

Tissue staining and microscopy

For the studies performed on frozen tissue sections, mice were anesthetized and the tissues were fixed by vascular perfusion of 1% paraformaldehyde in PBS pH 7.4 for 4 minutes under 120 mm/Hg of pressure. GC muscles were harvested, post fixed in 0.5% paraformaldehyde in PBS for 2 hours, cryo-protected in 30% sucrose in PBS overnight at 4°C, embedded in OCT compound (CellPath, Newtown, Powys, UK), frozen in freezing isopentane and cryosectioned. Cryosections were obtained systematically in a caudo-rostral direction throughout the whole sample, maintaining an anatomically standardized orientation, and analyses were performed on all sections representing the complete area of implantation. Tissue sections (30 µm) were stained with Hematoxylin and eosin (H&E) and in addition, the gel biocompatibility was examined with Masson trichrome staining (Réactifs RAL, Martillac, France), performed according to manufacturer's instructions. For immunofluorescent staining of neighboring 30 µm thick longitudinal cryosections, the sections were blocked with PBS 0.1% triton supplemented with 5% normal goat or donkey serum and 2% BSA (all reagents from Sigma-Aldrich Chemie GmbH, Steinheim, Germany) for 1 hour. The slides were then incubated for 1.5 hour at room temperature with the following primary antibodies and dilutions: rat anti-mouse PECAM-1 (clone MEC 13.3, BD Biosciences, Basel, Switzerland) at 1:100 or hamster monoclonal anti-mouse CD31 (clone 2H8, Millipore, Merck, Germany) at 1:200; mouse anti-mouse/human α-SMA (clone 1A4, MP Biomedicals, Basel, Switzerland) at 1:400; anti-mouse

NG2 (Chemicon International, Hampshire, UK) at 1:200; rabbit anti-Ki67 (Abcam, Cambridge, UK) at 1:100; rat monoclonal anti-CD11b (clone M1/70, Abcam, Cambridge, UK) at 1:100; rat anti-mouse CD45 (PE conjugated, clone 30 F11, BD Biosciences, Basel, Switzerland) at 1:400. Negative controls lacking primary antibody were always performed. Sections were rinsed in PBS 0.1% triton and then incubated for 1.5 hour at room temperature with fluorescently labeled secondary antibodies (Invitrogen, Basel, Switzerland) diluted at 1:200. The slides were then rinsed and mounted.

Piezo1 staining immunohistochemistry experiments were performed on Ventana DiscoveryUltra instrument (Roche Diagnostics, Manheim, Germany) by using the procedure RUO Discovery Universal instead. Cryosections were fixed for 12 minutes with 4% paraformaldehyde followed by 1 hour incubation at 37°C with rat anti-CD11b (1:100), alone or together with rat monoclonal anti-CD115 (clone CSF-1R, Biolegend, London, UK) at 1:100 or rat monoclonal anti-Ly6G (clone 1A8, Biolegend, London, UK) at 1:100, and 32 minutes incubation at 37°C with fluorescently labeled anti-rat IgG1 or IgG2a secondary antibodies used at 1:100 (ThermoFisher Scientific, Basel, Switzerland). Next, after an antibody denaturation step, sections were pre-treated for 16 minutes with Cell Conditioning Solution (CC1) (Roche Diagnostics, Mannheim). Rabbit anti-Piezo1 (Proteintech, Manchester, UK) diluted at 1:500 was then incubated for 32 minutes at 37°C and detected with the secondary antibody (ImmPRESS reagent kit peroxidase anti-rabbit Ig MP-7401, Vector Laboratories, Burlingame, CA, USA) applied manually (200 µl) for 32 minutes. Discovery Rhodamine (Roche Diagnostics, Mannheim) applied for 12 minutes was used for the detection. To study vessel perfusion, 100 µg of biotinylated Lycopersicon esculentum (tomato) lectin (Vector Laboratories, Burlingame, CA, USA) was dissolved in 100 µl, which binds the luminal surface of all blood vessels, and injected intravenously through the femoral vein. After four minutes the thoracic cavity was opened and the tissues were fixed by perfusing the animal with 1%

paraldehyde and leg muscle were collected and processed as described above. Fluorescently labeled Streptavidin (eBioscience, Vienna, Austria) at 1:200 was used to visualize the perfused vasculature. Frozen sections were mounted with Faramount Aqueous Mounting Medium (Dako, Agilent Technologies, Basel, Switzerland), and fluorescence images were taken with 40x objectives on a Carl Zeiss LSM710 3-laser scanning confocal microscope (Carl Zeiss, Feldbach, Switzerland) or with a 20X objective on an Olympus BX61 microscope (Olympus, Volketswil, Switzerland). All Image analysis were performed with either Cell Sense software (Olympus, Volketswil, Switzerland) or Imaris 7.6.5 software (Bitplane, Zürich, Switzerland) on fluorescence images acquired with a 20X objective on an Olympus BX61 microscope or with a 40x objective on a Carl Zeiss LSM710 3-laser scanning confocal microscope.

Histological analysis

The quantification of vessel length density (VLD) and vessel perfusion was performed on sections of leg muscles harvested after intravascular staining with biotinylated lectin and fluorescently labeled streptavidin, as described above. After co-staining with a fluorescent anti-CD31 antibody, VLD was measured on 6-10 randomly acquired fields per leg and 4 muscles per group (n = 4) by tracing the total length of vessels in the fields and dividing it by the area of the fields. The total lengths of lectin-positive and CD31-positive vascular structures in each field were traced independently and the vessel perfusion index was calculated as the ratio between the two values. The degree of branching of a vascular network depends on the total number of branch points in relation to the total amount of vascularity. Therefore, the degree of vessel branching was quantified by counting the number of branch points (n) in all representative fields per muscles and dividing the corresponding total vessel length by n+1, yielding the average vascular segment length. Vessel diameters were measured by overlaying a captured microscopic image with a square grid. Squares were chosen at random, and the

diameter of each vessel (if any) in the center of selected squares was measured. Two to five hundred total vessel diameter measurements were obtained from 4 muscles per each group (n = 4). The quantification of pericyte coverage was performed on sections of leg muscles after immunostaining for endothelium (CD31) and pericytes (NG2). The total lengths of CD31- and NG2-positive structures were measured by a blinded investigator and the pericyte coverage index was calculated as the ratio between the two values. Ki67$^+$ endothelial cells (ECs) were quantified from the total number of ECs (260-890 total ECs were counted per condition at 7 weeks post gel implantation) in vascular structures visible in each of 3-5 fields, in each area of effect. 10 areas with a clear angiogenic effect were analyzed per group. The quantification of leukocytes (CD45) and monocyte (CD11b) were performed on 7 random areas per muscle (n = 4) per group by counting them and normalizing to the absolute number of CD45$^+$ and CD11b$^+$ cells with area. (9000-1400 total CD45$^+$ cells and 5000-6000 total CD11$^+$ cells were counted per condition at 2 weeks post gel implantation). The quantification of Piezo1$^+$/CD11b$^+$ cells was performed on 7-10 random areas per muscle (n = 4 samples/group) after immunostaining for CD11b (700-800 total CD11$^+$ cells were counted per condition at 2 weeks post gel implantation). The quantification of Piezo1$^+$/CD11b$^+$/ CD115$^+$ monocytes and Piezo1$^+$/CD11b$^+$/Ly6G$^+$ neutrophils was performed on 5-7 random areas per muscle (n = 4 samples/group) after immunostaining for CD11b, CD115 or Ly6G (480-900 total CD11b$^+$ cells were counted per condition at 2 weeks post gel implantation).

All Image measurements were performed with both Cell Sense software (Olympus, Volketswil, Switzerland) and Imaris 7.6.5 software on fluorescence images acquired with a 20X objective on an Olympus BX61 microscope or with a 40x objective on a Carl Zeiss LSM710 3-laser scanning confocal microscope.

Blood cell analysis by FACS

Peripheral Blood Mononuclear Cells (PBMCs) were isolated from the whole blood of 4 immune-deficient SCID CB.17 mice (Charles River Laboratories, Sulzfeld, Germany) and 3 human healthy donor using a red blood cell lysis buffer (RBC Lysis Buffer, Invitrogen, Basel, Switzerland). After lysis, the PBMCs were stained with APC-anti-human CD11b (clone CBRM1/5, Biolegend, Basel, Switzerland) at 1:100, PE-anti-human CD66b (clone G10F5, Biolegend, Basel, Switzerland) at 1:100 and BV711-anti-human CD14 (clone M5E2, Biolegend, Basel, Switzerland) at 1:100, or BV605-anti-mouse-CD11b (clone M1/70, Biolegend, Basel, Switzerland) at 1:100, PE-anti-mouse-Ly6G (clone 1A8, BD Biosciences, Basel, Switzerland) at 1:100, APC-anti-mouse-CD115 (clone AFS98, BD Biosciences, Basel, Switzerland) at 1:100. A cross-reacting anti-human Piezo1 (Abcam, Cambridge, UK) was used at 1:500 for both human and mouse cells. An Alexa Fluor 488-labeled secondary antibody was used to detect Piezo1 (Invitrogen, Basel, Switzerland) at 1:200. Samples were acquired by LSR Fortessa (BD Biosciences, Basel, Switzerland), and data analyzed by FlowJo software (Tree Star, Ashland, OR, USA).

Statistical analysis

Data are presented as mean±standard error. All quantifications have been performed by blinded investigators to avoid bias. The significance of differences was assessed with the GraphPad Prism 7.03 software (GraphPad Software). The normal distribution of all data sets was tested and, depending on the results, multiple comparisons were performed with the parametric 1-way analysis of variance (ANOVA) followed by the Sidak test for multiple comparisons, or with the non-parametric Kruskal-Wallis test followed by Dunn's post-test, while single comparisons were analyzed with the non-parametric Mann-Whitney test or the parametric unpaired t-test.

Acknowledgements: This work was funded by the excellence initiative of the German Federal and State Governments Grant EXC 294 and Swiss National Foundation grant 163202 to A.B.

Author contribution: VPS and AF conceived the study. AF, RGB, AB and VPS designed the study. AF, RGB, AU, MS, EK, BF, MGM and SB carried out experiments, AF, RGB, AU, MS, KA, AB and VPS analyzed data, AF, RGB, MS, AB and VPS wrote the manuscript.

Competing Interests: VPS, AF, AB and RGB are listed as inventors in a patent application covering the use of CA in therapeutic angiogenesis.

References:

[1] S. Takeshita, L. P. Zheng, E. Brogi, M. Kearney, L. Q. Pu, S. Bunting, N. Ferrara, J. F. Symes, J. M. Isner, J Clin Invest 1994, 93, 662.
[2] J. K. Leach, D. Kaigler, Z. Wang, P. H. Krebsbach, D. J. Mooney, Biomaterials 2006, 27, 3249; E. A. Silva, D. J. Mooney, J Thromb Haemost 2007, 5, 590.
[3] F. W. Sellke, R. J. Laham, E. R. Edelman, J. D. Pearlman, M. Simons, Ann Thorac Surg 1998, 65, 1540; H. Hosseinkhani, M. Hosseinkhani, A. Khademhosseini, H. Kobayashi, Y. Tabata, Biomaterials 2006, 27, 5836; H. H. Chu, J. Gao, C. W. Chen, J. Huard, Y. D. Wang, Proc. Natl Acad Sci USA 2011, 108, 13444.
[4] T. Asahara, T. Murohara, A. Sullivan, M. Silver, R. van der Zee, T. Li, B. Witzenbichler, G. Schatteman, J. M. Isner, Science 1997, 275, 964; S. Kaushal, G. E. Amiel, K. J. Guleserian, O. M. Shapira, T. Perry, F. W. Sutherland, E. Rabkin, A. M. Moran, F. J. Schoen, A. Atala, S. Soker, J. Bischoff, J. E. Mayer, Nat Med 2001, 7, 1035.
[5] M. L. Springer, G. Hortelano, D. M. Bouley, J. Wong, P. E. Kraft, H. M. Blau, J Gene Med 2000, 2, 279; A. Banfi, G. von Degenfeld, R. Gianni-Barrera, S. Reginato, M. J. Merchant, D. M. McDonald, H. M. Blau, Faseb J 2012, 26, 2486.
[6] J. M. Isner, K. Walsh, J. Symes, A. Pieczek, S. Takeshita, J. Lowry, S. Rossow, K. Rosenfield, L. Weir, E. Brogi, et al., Circulation 1995, 91, 2687; D. W. Losordo, P. R. Vale, J. F. Symes, C. H. Dunnington, D. D. Esakof, M. Maysky, A. B. Ashare, K. Lathi, J. M. Isner, Circulation 1998, 98, 2800; T. T. Rissanen, I. Vajanto, S. Yla-Herttuala, Eur J Clin Invest 2001, 31, 651; M. Giacca, S. Zacchigna, Gene Ther 2012, 19, 622.
[7] M. Kubo, T. S. Li, R. Suzuki, B. Shirasawa, N. Morikage, M. Ohshima, S. L. Qin, K. Hamano, Am J Physiol-Heart C 2008, 294, H590; T. S. Li, K. Hamano, K. Suzuki, H. Ito, N. Zempo, M. Matsuzaki, Am J Physiol Heart Circ Physiol 2002, 283, H468; M. Kubo, T. S. Li, H. Kurazumi, Y. Takemoto, M. Ohshima, K. Hamano, Circulation 2011, 124.

[8] C. R. Ozawa, A. Banfi, N. L. Glazer, G. Thurston, M. L. Springer, P. E. Kraft, D. M. McDonald, H. M. Blau, J Clin Invest 2004, 113, 516.
[9] G. Bergers, S. Song, Neuro Oncol 2005, 7, 452.
[10] M. Murakami, Int J Vasc Med 2012, 2012, 293641; M. S. Wietecha, W. L. Cerny, L. A. DiPietro, Curr Top Microbiol 2013, 367, 3.
[11] N. Koike, D. Fukumura, O. Gralla, P. Au, J. S. Schechner, R. K. Jain, Nature 2004, 428, 138; P. Au, J. Tam, D. Fukumura, R. K. Jain, Blood 2008, 111, 4551.
[12] A. C. Newman, M. N. Nakatsu, W. Chou, P. D. Gershon, C. C. W. Hughes, Mol Biol Cell 2011, 22, 3791.
[13] C. J. Avraamides, B. Garmy-Susini, J. A. Varner, Nat Rev Cancer 2008, 8, 604.
[14] S. H. Kim, J. Turnbull, S. Guimond, J Endocrinol 2011, 209, 139.
[15] D. E. Ingber, P Natl Acad Sci USA 1990, 87, 3579.
[16] A. Forget, J. Christensen, S. Ludeke, E. Kohler, S. Tobias, M. Matloubi, R. Thomann, V. P. Shastri, P Natl Acad Sci USA 2013, 110, 12887.
[17] E. J. Chen, J. Novakofski, W. K. Jenkins, W. D. OBrien, Ieee T Ultrason Ferr 1996, 43, 191; K. Lima, J. F. S. Costa Junior, W. C. A. Pereira, L. F. Oliveira, Ultrasonography 2018, 37, 3.
[18] M. D. Bale, M. F. Muller, J. D. Ferry, Biopolymers 1985, 24, 461.
[19] A. J. LeBlanc, L. Krishnan, C. J. Sullivan, S. K. Williams, J. B. Hoying, Microcirculation 2012, 19, 676.
[20] M. L. Ponce, Methods Mol Biol 2009, 467, 183; K. M. Malinda, Methods Mol Biol 2009, 467, 287.
[21] K. Gaengel, G. Genove, A. Armulik, C. Betsholtz, Arterioscler Thromb Vasc Biol 2009, 29, 630.
[22] E. Groppa, S. Brkic, E. Bovo, S. Reginato, V. Sacchi, N. Di Maggio, M. G. Muraro, D. Calabrese, M. Heberer, R. Gianni-Barrera, A. Banfi, EMBO Mol Med 2015, 7, 1366.
[23] W. W. Yuen, N. R. Du, C. H. Chan, E. A. Silva, D. J. Mooney, Proc Natl Acad Sci U S A 2010, 107, 17933.
[24] M. Potente, H. Gerhardt, P. Carmeliet, Cell 2011, 146, 873.
[25] T. Scholzen, J. Gerdes, J Cell Physiol 2000, 182, 311.
[26] R. Gianni-Barrera, M. Trani, C. Fontanellaz, M. Heberer, V. Djonov, R. Hlushchuk, A. Banfi, Angiogenesis 2013, 16, 123.
[27] C. Murdoch, M. Muthana, S. B. Coffelt, C. E. Lewis, Nat Rev Cancer 2008, 8, 618.
[28] S. Zacchigna, L. Pattarini, L. Zentilin, S. Moimas, A. Carrer, M. Sinigaglia, N. Arsic, S. Tafuro, G. Sinagra, M. Giacca, J Clin Invest 2008, 118, 2062.
[29] N. R. Blumenthal, O. Hermanson, B. Heimrich, V. P. Shastri, Proc Natl Acad Sci U S A 2014, 111, 16124.
[30] S. M. Weis, D. A. Cheresh, Cold Spring Harb Perspect Med 2011, 1, a006478.
[31] B. Nilius, EMBO Rep 2010, 11, 902.
[32] J. Li, B. Hou, S. Tumova, K. Muraki, A. Bruns, M. J. Ludlow, A. Sedo, A. J. Hyman, L. McKeown, R. S. Young, N. Y. Yuldasheva, Y. Majeed, L. A. Wilson, B. Rode, M. A. Bailey, H. R. Kim, Z. Fu, D. A. Carter, J. Bilton, H. Imrie, P. Ajuh, T. N. Dear, R. M. Cubbon, M. T. Kearney, R. K. Prasad, P. C. Evans, J. F. Ainscough, D. J. Beech, Nature 2014, 515, 279; S. S. Ranade, Z. Z. Qiu, S. H. Woo, S. S. Hur, S. E. Murthy, S. M. Cahalan, J. Xu, J. Mathur, M. Bandell, B. Coste, Y. S. J. Li, S. Chien, A. Patapoutian, P Natl Acad Sci USA 2014, 111, 10347.
[33] R. Syeda, M. N. Florendo, C. D. Cox, J. M. Kefauver, J. S. Santos, B. Martinac, A. Patapoutian, Cell Rep 2016, 17, 1739.

[34] S. Jhunjhunwala, S. Aresta-DaSilva, K. Tang, D. Alvarez, M. J. Webber, B. C. Tang, D. M. Lavin, O. Veiseh, J. C. Doloff, S. Bose, A. Vegas, M. Ma, G. Sahay, A. Chiu, A. Bader, E. Langan, S. Siebert, J. Li, D. L. Greiner, P. E. Newburger, U. H. von Andrian, R. Langer, D. G. Anderson, Plos One 2015, 10, e0137550.
[35] B. N. Jaeger, J. Donadieu, C. Cognet, C. Bernat, D. Ordonez-Rueda, V. Barlogis, N. Mahlaoui, A. Fenis, E. Narni-Mancinelli, B. Beaupain, C. Bellanne-Chantelot, M. Bajenoff, B. Malissen, M. Malissen, E. Vivier, S. Ugolini, J Exp Med 2012, 209, 565.
[36] K. Sadtler, K. Estrellas, B. W. Allen, M. T. Wolf, H. Fan, A. J. Tam, C. H. Patel, B. S. Luber, H. Wang, K. R. Wagner, J. D. Powell, F. Housseau, D. M. Pardoll, J. H. Elisseeff, Science 2016, 352, 366.
[37] B. D. Medoff, E. Seung, S. Hong, S. Y. Thomas, B. P. Sandall, J. S. Duffield, D. A. Kuperman, D. J. Erle, A. D. Luster, J Immunol 2009, 182, 623.

Figures

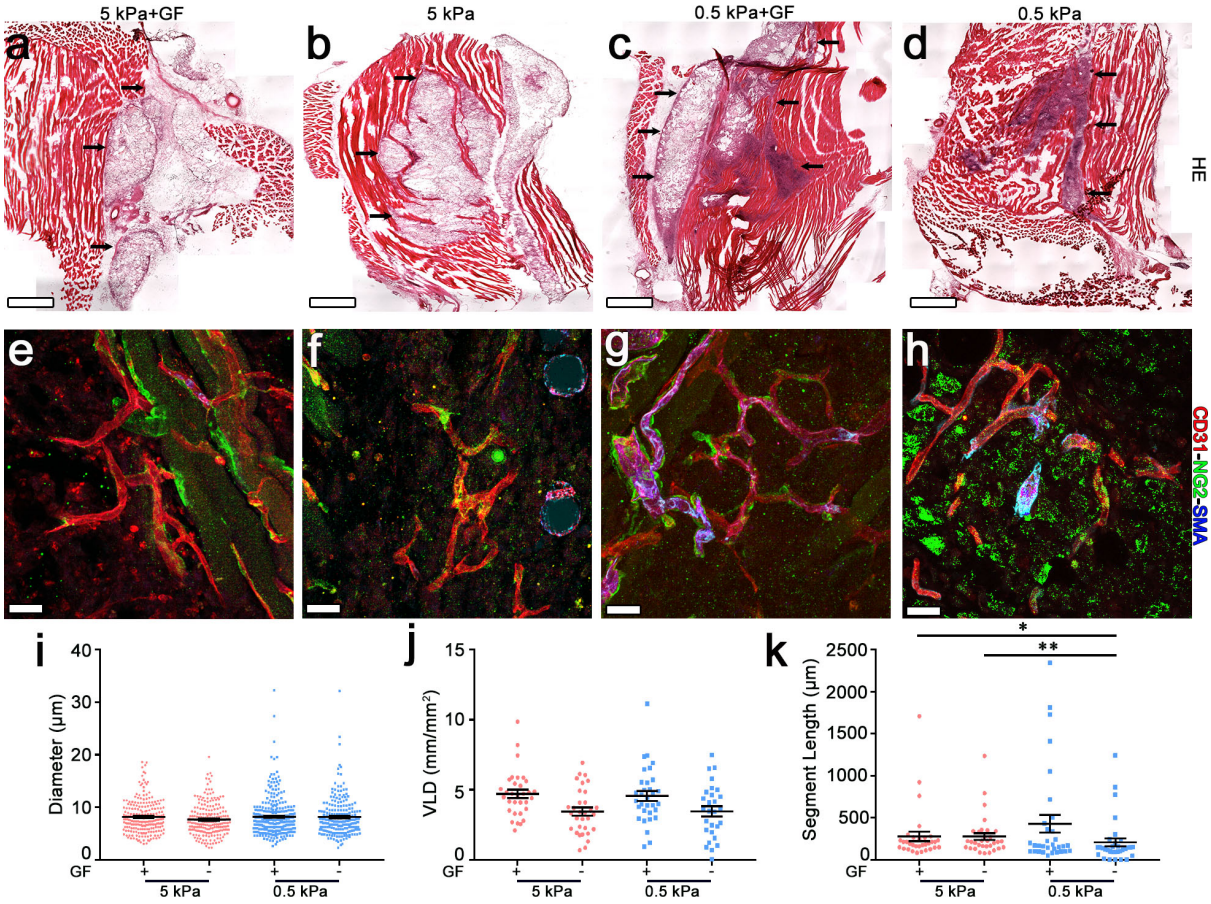

Figure 1. RGD functionalized carboxylated agarose hydrogels induce angiogenesis. a-d Frozen sections of GC muscles, implanted with distinct hydrogel compositions and harvested 2 weeks later, were stained for hematoxylin/eosin and **(e-h)** immunostained against CD31 (endothelial cells, red), NG2 (pericytes, green), α-SMA (smooth muscle cells, cyan). Black arrows in **a-d** indicate the injected gels. Quantification of vessel morphology: Vessel diameters (**i**) and vascular segment length (**j**) were quantified in the same areas within the hydrogels two weeks post implantation: VLD = vessel length density, is expressed as millimeters of vessel length per square millimeter of area of effect (mm/mm^2); the segment length is expressed as µm of vessel length between 2 consecutive branch points **(k)**. GF=Growth Factors. All data sets represent mean values ± SEM with all individual measurements shown; * $p<0.05$, ** $p<0.01$ by Kruskal-Wallis test; n= 4 independent muscles per each group. Scale bars = 1 mm in all HE-stained panels. Scale bars = 20 µm in all immunofluorescence-stained panels.

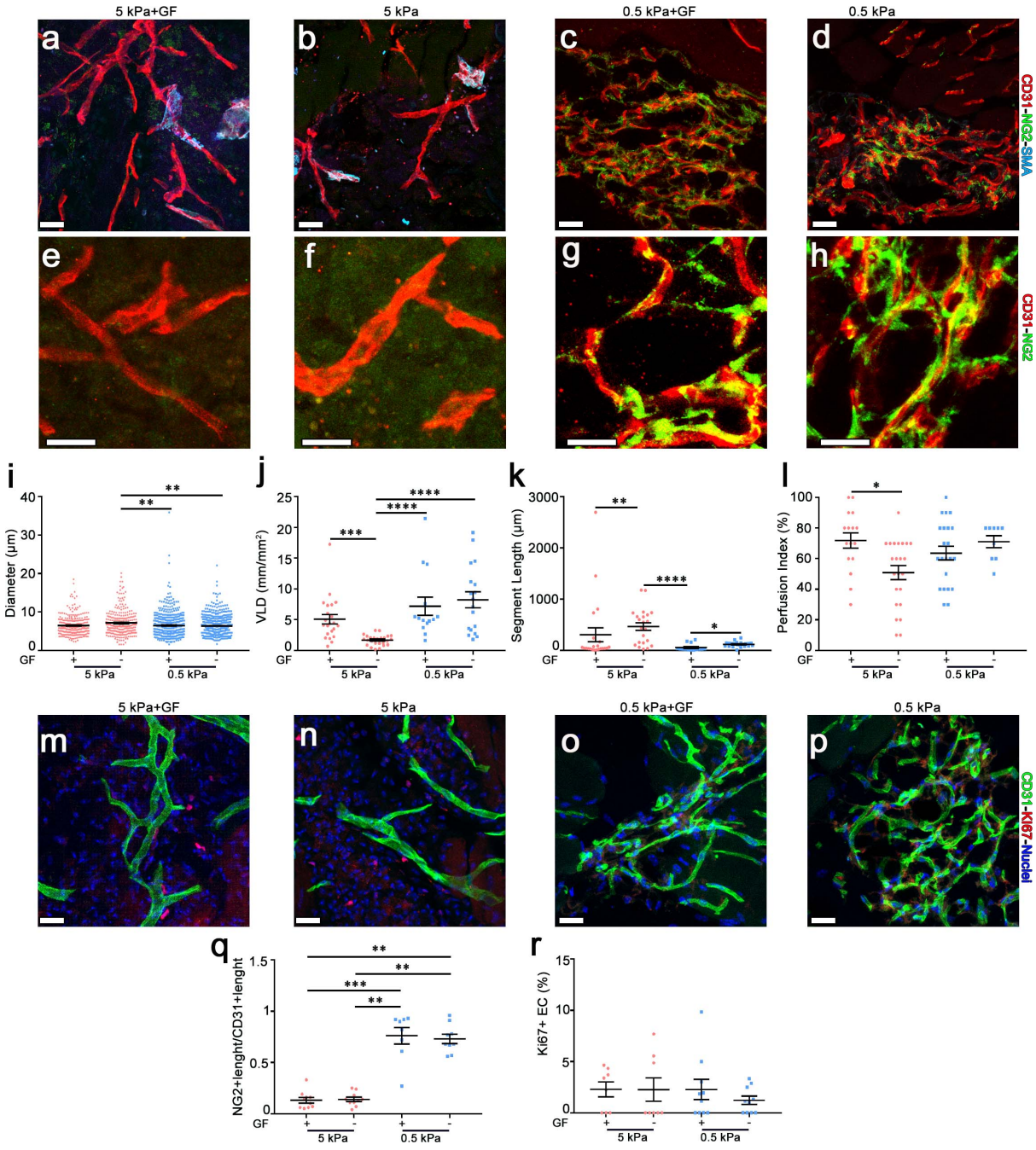

Figure 2. Soft RGD-functionalized carboxylated agarose supports stable capillaries. a-h Immunofluorescence staining of endothelium (CD31, in red), pericytes (NG2, in green), smooth muscle cell (α-SMA, in cyan) on frozen sections of leg skeletal muscles of mice injected with distinct hydrogel compositions and sacrificed 7 weeks later. Higher-magnification panels (**e-h**) show the tight association between pericytes and endothelium of vessels in soft gels (**g-h**). **i-l** VLD, vascular segment length, vessel diameters and perfusion index were quantified in the same areas within the hydrogels. GF=Growth Factors. All data sets represent mean values ± SEM with all individual measurements

shown; * p<0.05, ** p<0.01, *** p<0.001 and ****p<0.0001 by Kruskal-Wallis test; n= 4 independent muscles per each group. **m-p**, **r** Endothelial proliferation was assessed by quantifying the percentage of endothelial cells positive for Ki67 **(r)** by immunofluorescence staining on frozen muscle sections (**m-p**), n= 4 independent muscles per group. **q** Pericyte coverage was quantified in areas implanted with each hydrogel. Soft gels displayed a marked increase in pericyte coverage compared to stiff gels. Data represent mean values ± SEM; ** p<0.01 and *** p<0.001 by Kruskal-Wallis test. n = 4 independent muscles per each group. Scale bars = 20 µm in all immunofluorescence-stained panels.

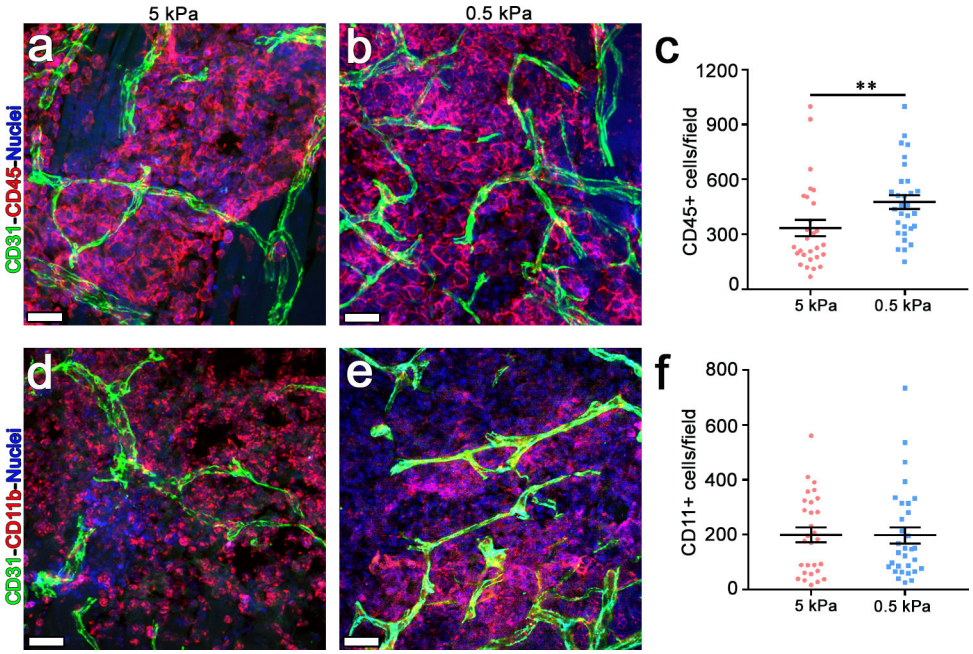

Figure 3. RGD Functionalized carboxylated agarose recruit myeloid cells. a, b, d, e Immunofluorescence staining of endothelial cells (CD31, in green), leukocyte (CD45, in red) and monocytes (CD11b, in red) on cryosections of limb muscles 2 week after injection with 5 kPa and 0.5 kPa hydrogel compositions. Scale bar= 20µm in all panels. **c, f** Quantification of the number of CD45+ and CD11b+ cells recruited into the implanted hydrogel. All data sets represent mean values ± SEM with all individual measurements shown; ** p<0.01, by Mann-Whitney test; n= 4 independent muscles per each group.

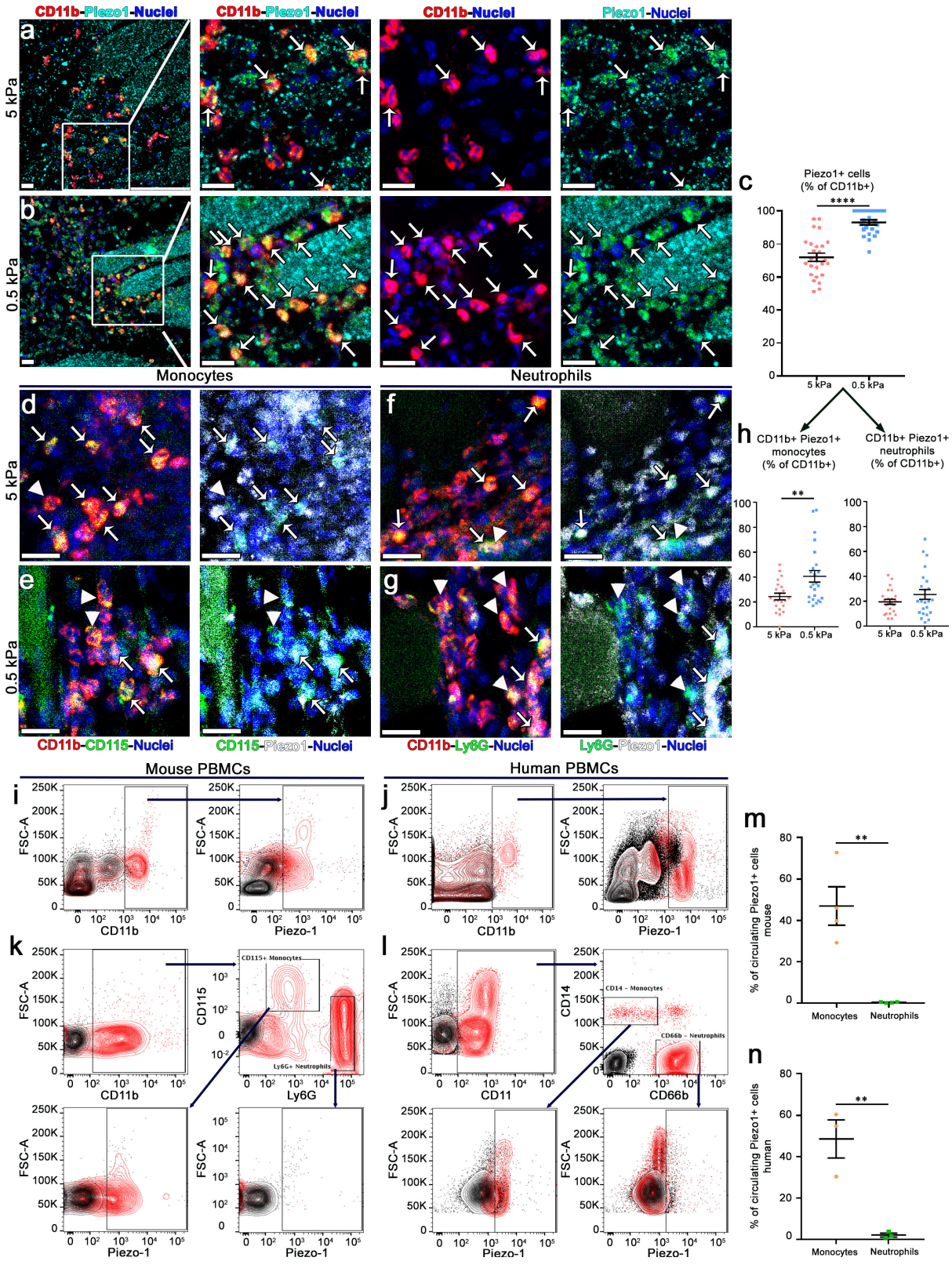

Figure 4. CD11b$^+$/CD115$^+$/Piezo-1$^+$ monocytes are enriched in soft RGD-functionalized carboxylated agarose microenvironment. (a-b) Immunofluorescence staining of CD11b$^+$ cells (in red) and of PIEZO-1$^+$ cells (in light blue) on cryosections of limb muscles 2 weeks after injection

with 5 kPa and 0.5 kPa hydrogel compositions. Scale bar= 20µm in all panels. (**c)** Quantification of $CD11b^+/Piezo1^+$ cells in sites within the implanted gels (% of total $CD11b^+$ cells). **(d-g)** Immunofluorescence staining of CD11b (in red), CD115 (in green), Ly6G (in green) and PIEZO-1 (in white) on cryosections of limb muscles. White arrows and arrowheads in panels **d** and **e** indicate Piezo-1^+ and Piezo-1^- monocytes ($CD11b^+/CD115^+$) respectively. White arrows and arrowheads in panels **f** and **g** similarly indicate Piezo-1^+ and Piezo-1^- neutrophils ($CD11b^+/Ly6G^+$) respectively. Scale bar= 20µm in all panels. (**h)** Quantification of $Piezo1^+$ monocytes and $Piezo1^+$ neutrophils in sites within the implanted gels (% of total $CD11b^+$ cells). **(i-j)** Circulating Piezo-$1^+/CD11b^+$ cells were identified in both mouse and human blood by FACS. (**k)** Detection of circulating Piezo-1^+ monocytes ($CD11b^+/CD115^+/Ly6G^-$) and neutrophils ($CD11b^+/CD115^-/Ly6G^+$) in mouse blood. (**l)** Detection of circulating Piezo-1^+ monocytes ($CD11b^+/CD14^+/CD66b^-$) and neutrophils ($CD11b^+/CD14^-/CD66b^+$) in human blood. (**m-n)** Quantification of circulating Piezo-1^+ monocytes and Piezo-1^+ neutrophils in mouse and human blood respectively (% of total monocytes or neutrophils). All data sets represent mean values ± SEM with all individual measurements shown; **** $p<0.0001$ and ** $p<0.01$ by unpaired t-test (**c**) or by Mann-Whitney test (**h**, **m** and **n**). FACS experiment: n= 4 mice and n= 3 human donors.

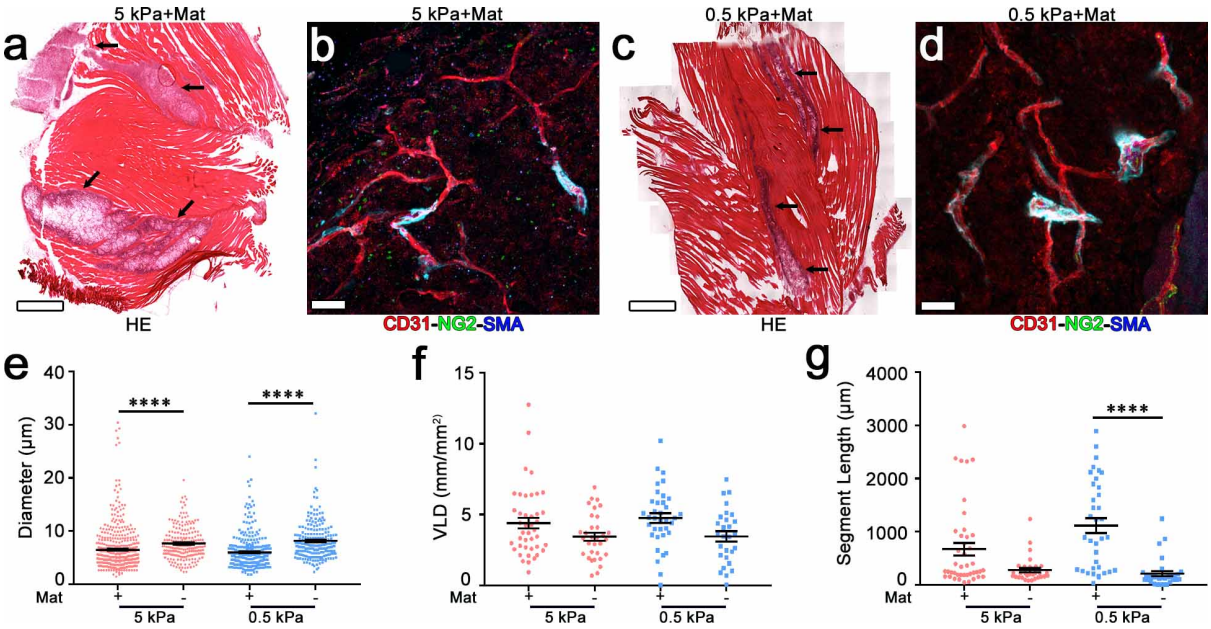

Supplemental Figure S1. Matrigel is not necessary to increase the vascular ingrowth inside the hydrogels. (**a-d)** Hind limb murine muscles were implanted with distinct hydrogel + Matrigel compositions. Two weeks later frozen sections were stained with hematoxylin/eosin (**a, c**) or immunostained against CD31 (endothelial cells, red), NG2 (pericytes, green) and α-SMA (smooth muscle cells, cyan) (**b, d**). Black arrows in **a** and **c** indicate the injected gels. **(e-g**) Quantification of vessel morphology: Vessel diameters (**e**), amount of angiogenesis (**f**) and vascular segment length (**g**) were quantified in the same areas within the hydrogels: VLD = vessel length density. All data sets represent mean values ± SEM with all individual measurements shown; ****p<0.0001 by Kruskal-Wallis test; n= 4 independent muscles per each group. Scale bars = 1 mm in all HE-stained panels; 20 µm in all immunofluorescence-stained panels.

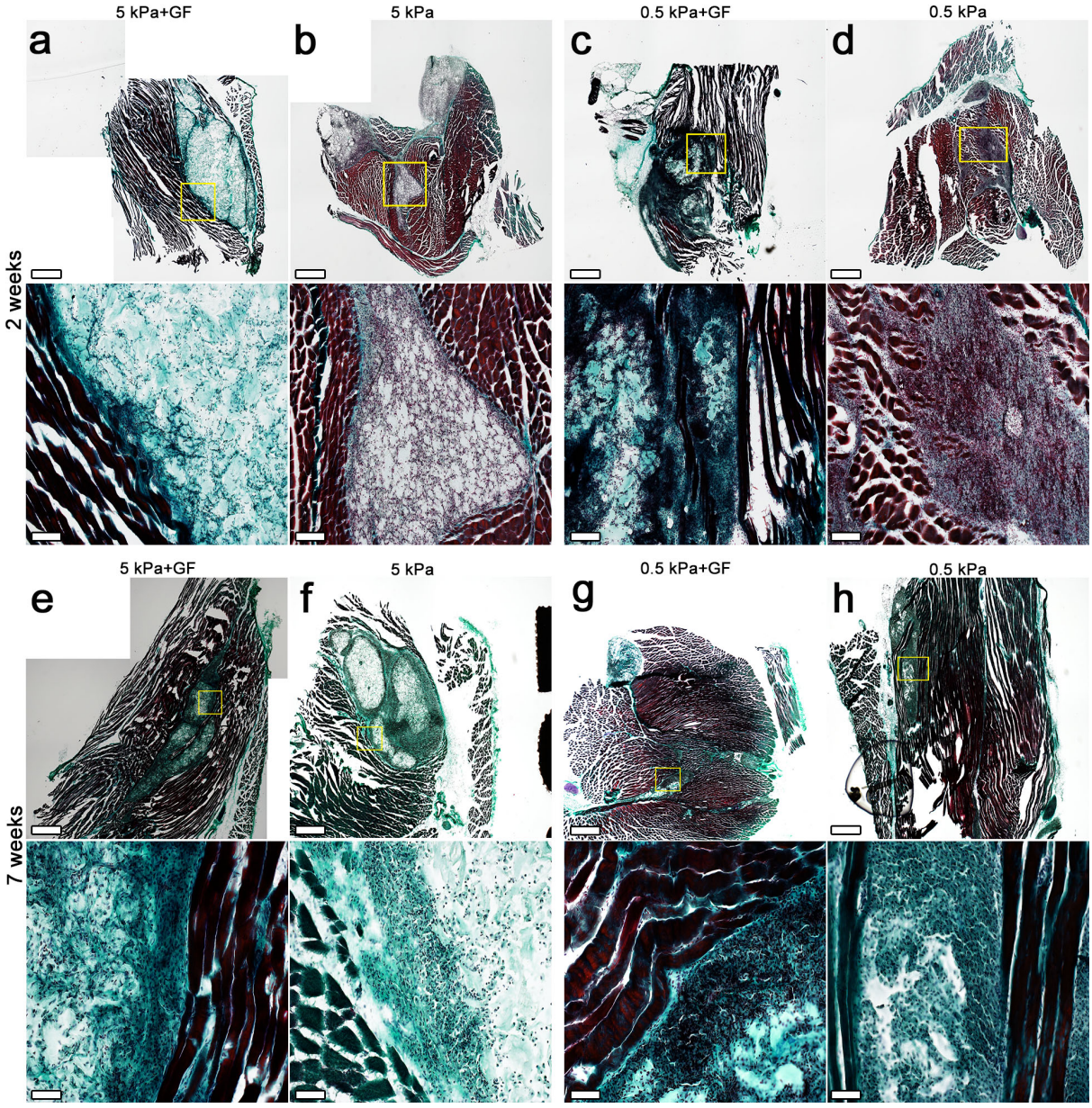

Supplemental Figure S2. RGD functionalized carboxylated agarose hydrogels are well integrated in muscle tissue. a-h Frozen sections of Gastrocnemius muscles implanted with distinct hydrogel compositions were stained for Masson trichrome staining. Two weeks (a-d) and 7 weeks (e-h) after implantation all hydrogels compositions were clearly persistent and well-integrated in muscle tissue. Lower panels represent higher-magnification images of the upper panels. n=4 independent muscles/group. Scale bars = 1 mm (low-magnification panels) and 50 μm (high-magnification panels).

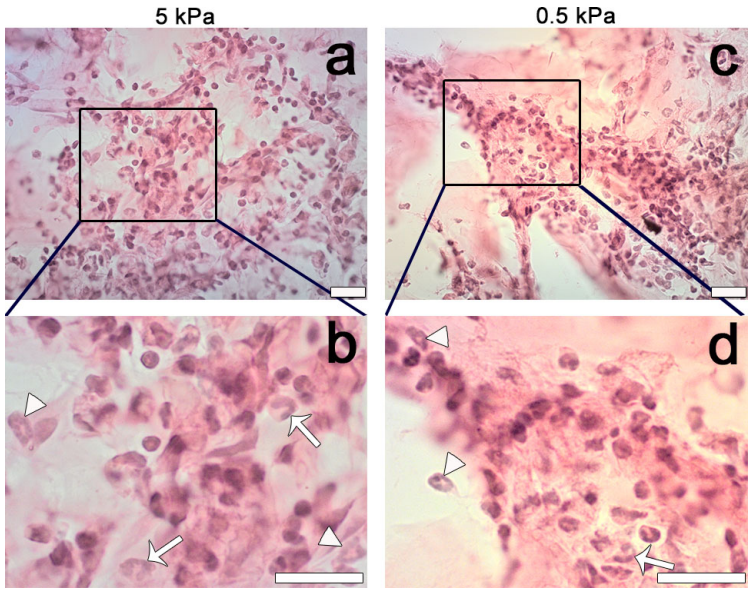

Supplemental Figure S3. Monocytes and neutrophils in sites within the implanted gels. H&E staining of cryosections of limb muscles 2 week after injection with 5 kPa (**a-b**) and 0.5 kPa hydrogel compositions (**c-d**). White arrows and arrowheads in high magnification panels (**b** and **d**) indicate monocytes and neutrophils, respectively. Scale bar = 20μm in all panels.